Journal of Power Sources 196 (2011) 6688–6694

Contents lists available at ScienceDirect

Journal of Power Sources

journal homepage: www.elsevier.com/locate/jpowsour

Challenges for rechargeable batteries

J.B. Goodenough*, Youngsik Kim[1]

Texas Materials Institute, ETC 9.184, The University of Texas at Austin, 1 University Station, C2201, Austin, TX 78712, USA

ARTICLE INFO

Article history:
Received 6 October 2010
Received in revised form
12 November 2010
Accepted 15 November 2010
Available online 3 December 2010

Keywords:
Insertion compounds
Liquid cathodes
Solid electrolytes

ABSTRACT

Strategies for Li-ion batteries that are based on lithium-insertion compounds as cathodes are limited by the capacities of the cathode materials and by the safe charging rates for Li transport across a passivating SEI layer on a carbon-based anode. With these strategies, it is difficult to meet the commercial constraints on Li-ion batteries for plug-in-hybrid and all-electric vehicles as well as those for stationary electrical energy storage (EES) in a grid.

Existing alternative strategies include a gaseous O_2 electrode in a Li/air battery and a solid sulfur (S_8) cathode in a Li/S battery. We compare the projected energy densities and EES efficiencies of these cells with those of a third alternative, a Li/Fe(III)/Fe(II) cell containing a redox couple in an aqueous solution as the cathode. Preliminary measurements indicate proof of concept, but implementation of this strategy requires identification of a suitable Li^+-ion electrolyte.

1. Introduction

The primary commercial targets for rechargeable batteries are: (1) portable electronics, (2) power tools and electric vehicles (EVs), and (3) stationary electrical energy storage (EES) for a grid supplied by wind, radiant-solar, and nuclear power. The first of these targets has already been realized commercially by the advent of the Li-ion rechargeable battery, and Li-ion batteries for power tools and small EVs are under active commercial development. The principal remaining challenge is to develop safe, rechargeable batteries for larger plug-in hybrid and all-electric vehicles (PHEVs and EVs) of larger driving range, faster charging rates, and lower cost as well as for EES for the grid.

A battery converts chemical energy stored in its two electrodes (the anode is the reductant and the cathode is the oxidant) into a discharge electronic current $I = I_{dis}$ at a voltage $V = V_{dis}$ for a time $\Delta t = \Delta t_{dis}$, and a rechargeable battery restores the chemical energy by the application of a charging current I_{ch} at a voltage V_{ch} over a time Δt_{ch}. The capacity of a battery delivering a current I_{dis} is the total amount of electronic charge $Q(I)$ transported to the cathode over the time Δt_{dis} for a complete discharge of the chemical energy available at I_{dis}. Resistances R_b to transport of the working ion (H^+, Li^+, or Na^+) across the electrode/electrolyte interfaces and within the electrolyte and any insertion-compound electrodes give a voltage loss $IR_b = \eta = V_{OC} - V$, where the open-circuit voltage $V_{OC} = (\mu_A - \mu_C)/e$ is the difference of separated anode and cathode electrochemical potentials and e is the magnitude of the electronic charge. At $I = 0$, transport of the working ion inside the cell of a battery from the anode to the cathode is not charge-compensated by an externally delivered electronic charge, so a positive potential is created at the cathode and a negative potential at the anode until the internal electric field prevents further flow of the working ion. The battery parameters of primary interest are, therefore, its

- maximum specific power output $I_m V_m$/wt ($W\,kg^{-1}$ or $mW\,g^{-1}$);
- specific capacity $Q(I)$/wt ($Ah\,kg^{-1}$ or $mAh\,g^{-1}$) where $Q = \int_0^{\Delta t} I dt = \int_0^Q dq$;
- specific and volumetric energy densities $\int_0^Q V(q)dq$/wt and $\int_0^Q V(q)dq$/vol ($W\,kg^{-1}$ or $mW\,g^{-1}$ and $Wh\,L^{-1}$);
- cycle life (number of charge/discharge cycles at which $Q(I)$ retains 80% of its initial value) and calendar life;
- polarization $\eta = V_{OC} - V(q,t)$;
- percent efficiency of EES at a given I, $(100 \times \int_0^Q V_{dis}dq / \int_0^Q V_{ch}dq)$.

The commercial constraints of safety and cost apply to all applications, but the required energy density versus I, calendar and cycle life, EES efficiency, and response or charging times vary greatly between batteries for electronic devices, EVs, and grid EES. Present-day strategies for the Li-ion battery rely on liquid-carbonate electrolytes and insertion-compound cathodes. We need to address the limitations of these strategies relative to alternatives for batteries that power larger EVs and store electrical energy of the grid.

* Corresponding author at: Mechanical Engineering, The University of Texas at Austin, 204 E Dean Keeton, ETC 9.184, Austin, TX 78712, USA. Tel.: +1 512 471 1646; fax: +1 512 471 7681.
E-mail addresses: jgoodenough@mail.utexas.edu (J.B. Goodenough), yk35@iupui.edu (Y. Kim).
[1] Present address: Department of Mechanical Engineering, Indiana University-Purdue University Indianapolis, Indianapolis, IN 46202, USA.

0378-7753/$ – see front matter © 2010 Elsevier B.V. All rights reserved.
doi:10.1016/j.jpowsour.2010.11.074

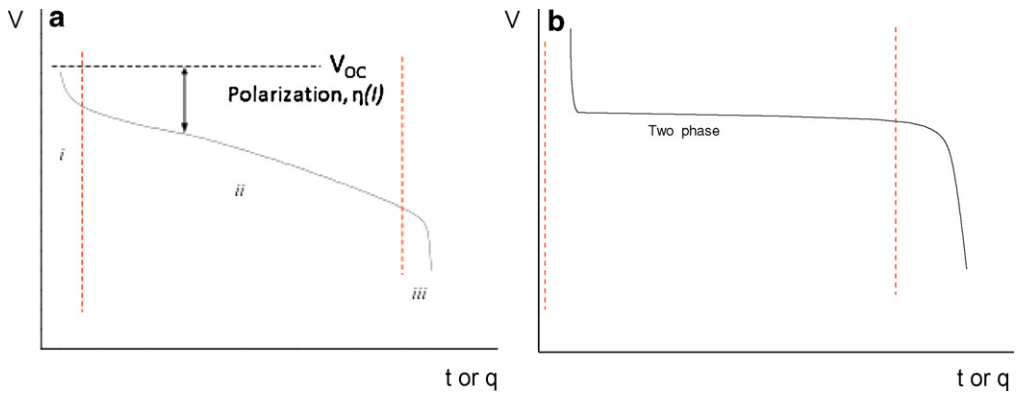

Fig. 1. Typical discharge V vs. t curves at a fixed I showing the polarization $\eta(I)$ for (a) a solid-state solution insertion reaction and (b) a two-phase reaction.

2. Limitations of existing strategies

2.1. Electrolytes

The "window" of an electrolyte, $E_g = E_{LUMO} - E_{HOMO}$ or $E_C - E_V$ is the energy difference between the lowest unoccupied and the highest occupied molecular orbitals (LUMO and HOMO) of a liquid electrolyte; between the bottom of the conduction band, E_C, and the top of the valence band, E_V, of an inorganic solid electrolyte. An anode with a $\mu_A > E_{LUMO}$ or E_C can transfer electrons to the LUMO or conduction band of the electrolyte, thereby reducing it; a cathode with a $\mu_C < E_{HOMO}$ or E_V can receive electrons from the electrolyte

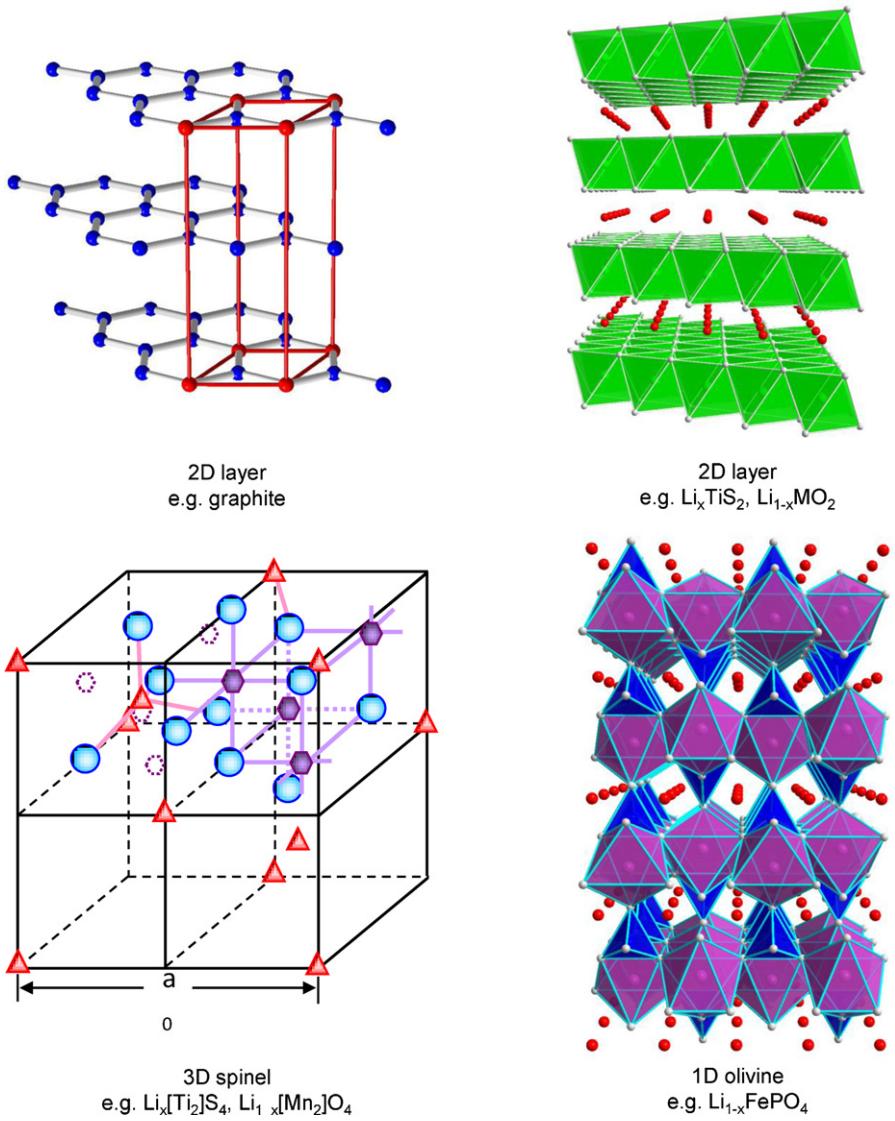

Fig. 2. Insertion-compound hosts with 2D, 3D, and 1D interstitial space for Li^+-ion transport.

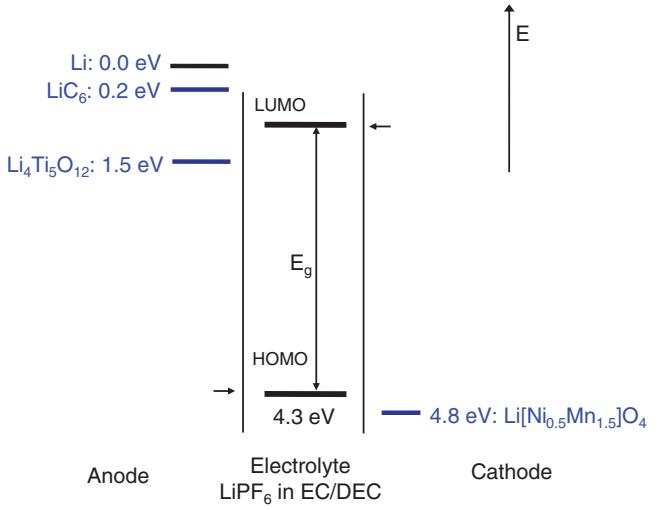

Fig. 3. Window of a liquid-carbonate electrolyte relative to the electrochemical potentials of LiC_6, $Li_4Ti_5O_{12}$ (LTO), and $Li[Ni_{0.5}Mn_{1.5}]O_4$ (LNMO).

to oxidize it. Water has an $E_g \approx 1.23$ eV, but formation of double layers at the electrode/aqueous-electrolyte interfaces can allow stability of 1.5 V in a cell with an aqueous electrolyte. The limited E_g of water has motivated the use of non-aqueous electrolytes, but at the expense of a lower working-ion conductivity than the $\sigma_H \approx 1\,S\,cm^{-1}$ of the H^+ ion in H_2SO_4 or KOH. Because of the volume changes of the electrodes during discharge and charge, it is normally advantageous to have a liquid or polymer–gel electrolyte with solid electrodes; but solid electrolytes have been used in all-solid microbatteries or where the electrodes are liquids, as in the Na/S battery.

Since H^+ ions are not sufficiently mobile in non-aqueous electrolytes, the Li^+ ion has been used as the working ion of a non-aqueous cell. The liquid carbonated can dissolve a sufficient concentration of Li salts to give a $\sigma_{Li} \approx 10^{-2}\,S\,cm^{-1}$, but the more viscous ionic liquids and the polyethylene-oxide (PEO) polymers have a disappointingly lower σ_{Li}, which is why most Li-ion batteries, especially the power batteries, use a liquid-carbonate electrolyte or a non-flammable blend containing a liquid-carbonate electrolyte. The liquid carbonates have an E_{LUMO} about 1.0 eV below the μ_A of a lithium anode, *i.e.*, the Li^+/Li^0 potential, and an E_{HOMO} about 4.3 eV below Li^+/Li^0. With carbon or a carbon-buffered alloy as the anode and ethylene carbonate (EC) as an additive to the liquid electrolyte, a passivating solid-electrolyte-interface (SEI) layer formed on the carbon [1] allows the use of an anode with a $\mu_A \approx 0.2$ eV versus Li^+/Li^0. However, the SEI layer consumes Li irreversibly on the initial charge of a Li-ion cell, which robs capacity from the cathode, unless the SEI layer is preformed before cell assembly. More important, insertion of Li across the SEI layer may be slower than the rate of plating of Li on the surface of the SEI layer during a fast charge, which limits the safe charging rate, unless a carbon buffered Li-alloy has a $\mu_A < \mu_{Li} - 0.7$ eV. This competition does not exist during discharge, so a fast discharge rate is safe. Plating out of Li results in dendrite formation; the dendrites grow on repeated cycling to where they can short-circuit a cell with dangerous consequences if the electrolyte is flammable. A battery with an electrolyte $\sigma_{Li} > 10^{-3}\,S\,cm^{-1}$ can limit the polarization loss sufficiently to allow design of a power battery, but it may be necessary to complement the battery for an EV with an electrochemical capacitor.

2.2. Electrodes

The solid electrodes of a conventional Li^+-ion battery are Li-insertion compounds. A Li-insertion compound consists of a host

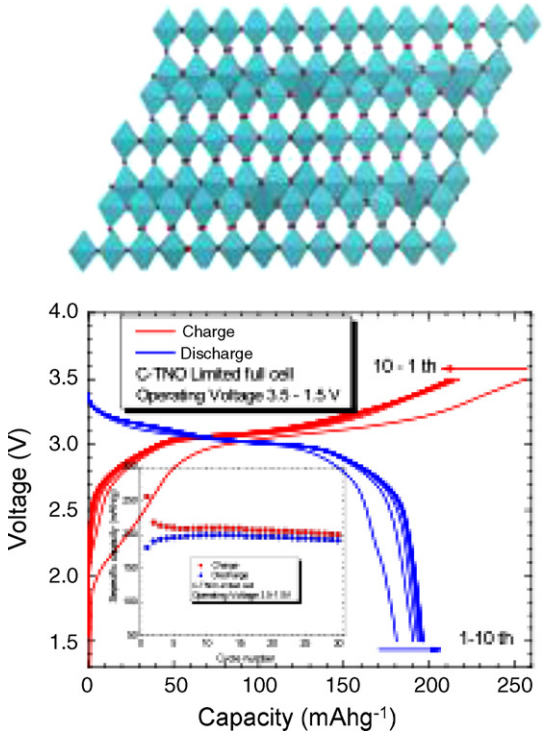

Fig. 4. Structure of $TiNb_2O_7$ (after M. Gasperin, [8]) and charge/discharge curves of a C-$TiNb_2O_7$/$Li[Ni_{0.5}Mn_{1.5}]O_4$ cell cycled between 1.5 and 3.5 V at C/10 rate together with its capacity retention over 30 cycles.
Courtesy of J.T. Han.

structure into which the guest, Li^+, can be inserted reversibly from the electrolyte; the Li^+ ions are charge-compensated by reduction of the host by electrons transferred from the other electrode via the external circuit. If, on discharge, the Li^+-ion insertion into a cathode and/or the Li^+-ion extraction from the anode is a solid-solution reaction, the voltage profile is as shown schematically in Fig. 1(a). In this profile for a full discharge, three polarization contributions are manifested. The diffusive ionic conductivities are

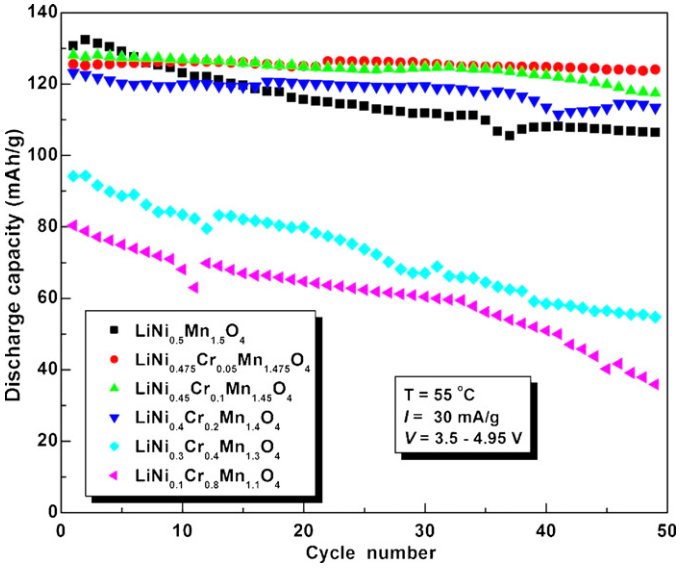

Fig. 5. $Li_{1-x}[Ni_{0.5-y}Cr_{2y}Mn_{1.5-y}]O_4$ capacity vs. cycle at 55 °C.
Courtesy of D.Q. Liu.

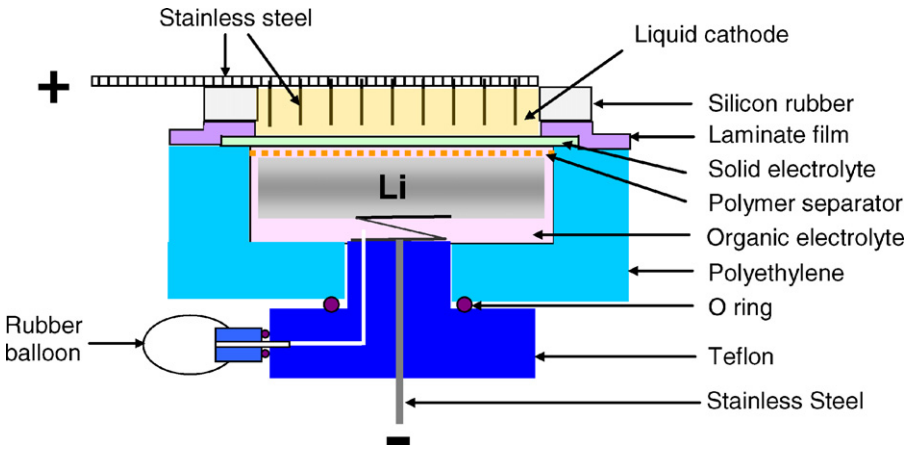

Fig. 6. Design of a Li/$Li_{1.3}Ti_{1.7}Al_{0.3}(PO_4)_3$/$Fe(NO_3)_3$/$Fe(NO_3)_2$ test cell.

$$\sigma_{Li} = \left(\frac{ne^2 D_{Li}}{kT}\right) \sim Nc(1-c)\exp\left(\frac{-\Delta H_m}{kT}\right) \quad (1)$$

where $n = Nc$ is the concentration of mobile Li^+ ions and c is the fraction of Li sites that are occupied in the electrodes (the $c(1-c)$ factor remains constant in the electrolyte, but not in the electrodes), D_{Li} is the Li^+-ion diffusion coefficient with a Li^+-ion motional enthalpy ΔH_m for each electrode and the electrolyte. On discharge, the ΔH_m for Li^+-ion transfer across the electrode/electrolyte interfaces and for Li^+-ion transfer in the electrolyte and the cathode introduces a sharp initial voltage drop in region (i); in region (ii), the continuing increase in η reflects changes in the μ_A and μ_C of the electrodes as well as of the electrode resistances; and at the end of discharge; region (iii), the small fraction c of occupied Li sites in the anode surface or of $(1-c)$ unoccupied Li sites in the cathode surface limits the rate of diffusion from the anode or into the cathode. The state of charge at which the surface of an electrode becomes diffusion limited increases as the current I_{dis} increases.

Fig. 1(b) shows the voltage profile where there is a two-phase displacement or insertion reaction. The constant voltage in the two-phase region is the consequence of the Gibbs phase rule.

The 2D Li insertion into layered hosts such as graphite or TiS_2, Fig. 2(a), was initially referred to as intercalation. The spinel host of Fig. 2(b) offers a 3D interstitial space for Li insertion/extraction with the transition-metal sites sharing only edges as in the layered oxides and TiS_2; $Li_{2x}[Ti_2]S_4$ with the spinel $[Ti_2]S_4$ framework gives an essentially identical discharge voltage profile as Li_xTiS_2 [2] since the Li^+ ions occupy only octahedral sites of this thiospinel framework. However, the discharge voltage profile (increasing x) of the oxospinel $Li_{2x}[Mn_2]O_4$ shows an abrupt drop of 1 V at $x = 0.5$ where the Li^+ ions are displaced in a cascade from the tetrahedral to the octahedral interstitial sites even though μ_C resides in the Mn(IV)/Mn(III) couple for all $0 \le x \le 1$. This site change limits the capacity of the $Li[M_2]O_4$ oxospinels to one per two M atoms. The ordered-olivine structure of $LiFePO_4$, Fig. 2(c), offers only 1D channels for a two-phase, reversible Li insertion into $FePO_4$ to $LiFePO_4$ at 3.45 V. Although the polyanion $(PO_4)^{3-}$ adds weight, nevertheless the specific capacity of Li_xFePO_4 is greater than that of the spinel $Li_{1-x}[Mn_2]O_4$ at 4.0 V to give a competitive energy density. Moreover, stabilization of $Li_{1-x}[Mn_2]O_4$ against Mn(II) dissolution on cycling [3], which is due to a surface disproportionation reaction, 2Mn(III) = Mn(II) + Mn(IV) [4], reduces further the capacity of $Li_{1-x}[Mn_2]O_4$. The fabrication of small $LiFePO_4$ particles coated and/or embedded in amorphous carbon or attached to a conductive polymer having an E_F at the energy of the cathode redox couple (*e.g.* polypyrrole or polyanaline with Li_xFePO_4 [5]) provides any needed electronic conductivity and a large enough surface area for fast Li insertion, *e.g.* a six-minute full discharge with only a limited loss of capacity. However, *the capacity of an insertion compound is limited by the concentration of Li that can be inserted reversibly into the host.*

Reversible displacement reactions can give a larger specific capacity than an insertion compound, but these reactions are plagued by large volume changes on cycling. Although alloys undergoing a displacement reaction can be used as anodes if buffered by carbon in a suitable composite morphology, nevertheless the problem of a safe rate of charge remains because of the SEI layer on the carbon. Therefore, safety considerations motivate the use of an anode having a $\mu_A < 1.0$ eV relative to Li^+/Li^0 in power batteries where a fast rate of charge is desired or V_{ch} remains too low for plating out of Li^0.

Fig. 3 illustrates the anode μ_A for Li, LiC_6, and the spinel $Li[Li_{1/3}Ti_{5/3}]O_4$ (LTO) relative to the LUMO of a liquid-carbonate electrolyte. Also shown is the μ_C of the spinel cathode $Li[Ni_{0.5}Mn_{1.5}]O_4$ (LNMO) relative to the HOMO; the decomposition energy of the electrolyte is *ca.* 5.0 eV below the Li^+/Li^0 μ_A. The LNMO cathode contains Mn(IV) only, which avoids complications associated with the Mn(III) ion. The LTO spinel has been shown [6] to be capable of a fast charge and discharge that is safe because it has a $\mu_A = 1.5$ V versus Li^+/Li^0, which is below the LUMO of the electrolyte. An alternative anode, $Ti_{0.9}Nb_{0.1}Nb_2O_7$, has also been shown [7] to give a safe and fast charge/discharge cycling for over 30 cycles over the voltage range $1.3 \le V \le 1.6$ V versus Li^+/Li^0 and to have a larger specific capacity of 300 mAh g^{-1} than the LTO spinel. Fig. 4 shows the structure of $TiNb_2O_7$ containing disordered Ti(IV) and Nb(V) ions [8] as well as the output voltage of a full cell with a carbon coated C-$TiNb_2O_7$ anode and an LNMO cathode with electrode masses giving a capacity Q limited by the anode. $TiNb_2O_7$ is an alternative host structure that demonstrates the Nb(V)/Nb(IV) as well as the Ti(IV)/Ti(III) couple can be used in an anode host oxide. In a full cell in which the capacity is limited by the LNMO cathode, the μ_C approaches 5.0 V versus Li^+/Li^0, and the capacity of the cell fades on cycling.

The voltage of a cell is limited not only by the intrinsic limit, E_g, of the electrolyte, but also by the intrinsic limits of the electrodes. If an anode is reduced during a charge by electrons entering an s orbital, a displacement reaction occurs as is illustrated with aqueous electrolytes in the anode reactions

$$Cd(OH)_2 + 2H^+ + 2e^- = Cd^0 + 2H_2O;$$
$$PbSO_4 + 2H^+ + 2e^- = Pb^0 + H_2SO_4 \quad (2)$$

The insertion-compound anodes of a Li^+-ion battery are reduced on charge by electrons entering either the d orbitals of a transition-metal host or the p_π orbitals of a layered compound like graphite.

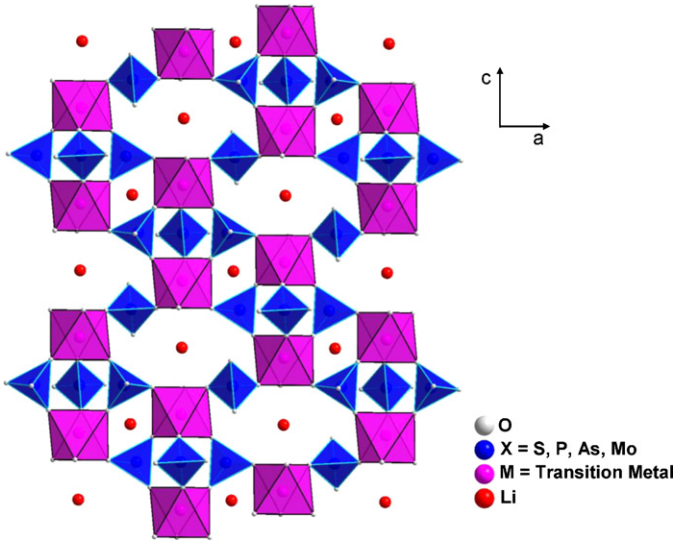

Fig. 7. Structure of $Li_{1.3}Ti_{1.7}Al_{0.3}(PO_4)_3$ with $\sigma_{Li} \approx 10^{-3}$ S cm^{-1} at room temperature.

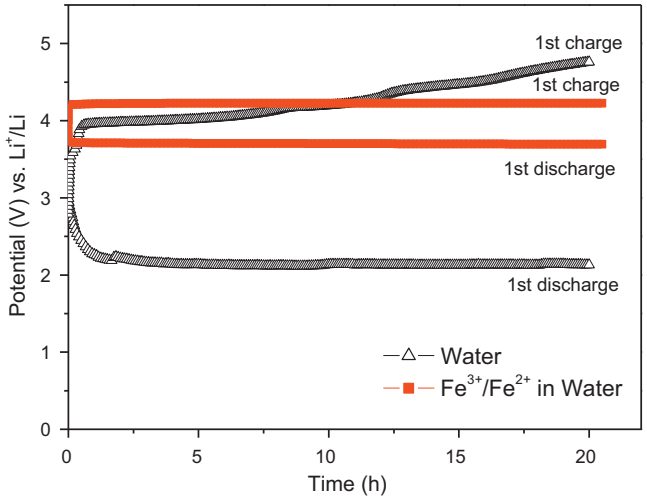

Fig. 8. Charge/discharge voltages of Li/H_2O and Li/$Fe(NO_3)_3$/Li/$Fe(NO_3)_2$ test cells.

Only the lighter elements of a *d*-block family, *e.g.* Ti, V, or Nb, have accessible *d* states below the bottom of an *s* conduction band that are at an energy of interest for an anode [9].

The voltage that can be achieved by an insertion-compound cathode is limited by the energy of the top of the host anion-*p* bands. This limit is about 2.7 eV below Li^+/Li^0 in layered $Li(V_{0.25}Cr_{0.75})S_2$ [10], which is why oxide hosts are used as cathodes [11]. As the energy of a redox couple is lowered across the top of the host anion-*p* bands, the *d*-state manifold is transformed from a redox couple to a band of strongly hybridized cation-*d* and anion-*p* itinerant-electron states of *d* symmetry, and the Fermi energy E_F becomes *pinned* in the antibonding states at an energy close to that of the top of the anion-*p* bands. As the cation-*d* states are lowered further relative to the anion-*p* states, the anion-*p* character of the itinerant-electron states increases until anion–anion *p* bonds are formed [10]. This transition occurs first at the surface of the cathode particles; it gives a flat voltage as it represents a new surface phase. This transition is exemplified in the layered cathode $Li_{1-x}CoO_2$, which begins to either evolve oxygen or insert H^+ from the electrolyte at $x > 0.55$ [12]. Where E_F is pinned at the top of an anion-*p* band, two formal mixed-valent cation states may be accessed without a voltage step between them, as has been demonstrated for V(V) to V(III) in layered $Li(V_{0.5}Cr_{0.5})S_2$ [10] and Ni(IV) to Ni(II) in layered $Li(Ni_{0.5}Mn_{0.5})O_2$ [13]. Of particular interest is the stabilization of the pinned E_F from about 4.0 eV below Li^+/Li^0 in the layered $Li_{1-x}(Co_yNi_{1-y})O_2$ oxides [14] to over 4.7 eV below Li^+/Li^0 in the presence of Mn(IV) in layered $Li_{1-x}(Ni_{0.5-y}Co_{2y}Mn_{0.5-y})O_2$ [15]. In the spinel $Li_{1-x}[Ni_{0.5}Mn_{1.5}]O_4$, the top of the O-2*p* bands appears to be about 5.0 eV below Li^+/Li^0, and reversible access to 4.8 eV below Li^+/Li^0 in $Li[Ni_{0.5-y}Cr_{2y}Mn_{1.5-y}]O_4$ is possible at 55 °C, Fig. 5, in spite of a $\mu_C < \mu_{HOMO}$ [16]. The Cr(III) moves Ni away from the surface to give a passivating SEI layer that is not formed by coating the surface with another oxide. A similar passivation has been achieved by the Manthiram group [17] by substitution of Fe rather than Cr. On the other hand, removal of Li from $Li[Ni_{0.5}Ti_{1.5}]O_4$ and $Li[CrTi]O_4$ is not reversible; but insertion of Li into these spinels at $V = 1.5$ V is reversible due to access to the Ti(IV)/Ti(III) couple [18]. Tuning of redox couples by changing a counter cation of a polyanion has also been demonstrated in the NASICON structure [19].

These examples and the 1 V step at $x = 0.5$ in $Li_{2x}[Mn_2]O_4$ reveal that redox couples and the top of the O-2*p* bands can be tuned by changes in structure and by changes of a counter cation; they also show that removal of the oxidizing species from the surface of a cathode particle by chemical substitution may prove a more efficient way to create a passivating SEI layer on a cathode than application of an oxide coat.

3. Alternative cathode strategies

Two alternative cathode strategies have been suggested: (1) use of gaseous O_2 in a Li/air battery [20] and (2) breaking of the S–S bonds of S_8 in a Li/S battery [21]. Both of these alternatives may require a Li^+-ion solid-electrolyte separator to enable use of a lithium-metal anode.

The Li/air cell depends on a catalyst for both the oxygen-reduction reaction (ORR) on discharge and also for the reverse oxygen-evolution reaction (OER) on charge: $2Li^+ + 2e^- + O_2 = Li_2O_2$. With α-$MnO_2$ as the catalyst, the ORR occurs at 2.75 V and the OER at 4.0 V versus Li^+/Li^0, which gives too poor an efficiency for EES; also catalytic activity limits the rates of discharge and charge. Even with the improved, but expensive Pt–Au alloy developed by the

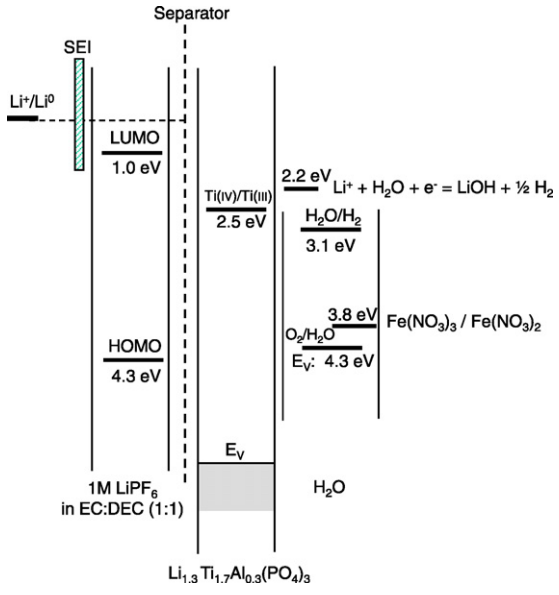

Fig. 9. Electrochemical potentials of the Li/liquid carbonate/$Li_{1.3}Ti_{1.7}Al_{0.3}(PO_4)_3$/$Fe(NO_3)_3$/$Fe(NO_3)_2$ in water and of the reaction $Li^+ + H_2O + e^- = LiOH + ½H_2$.

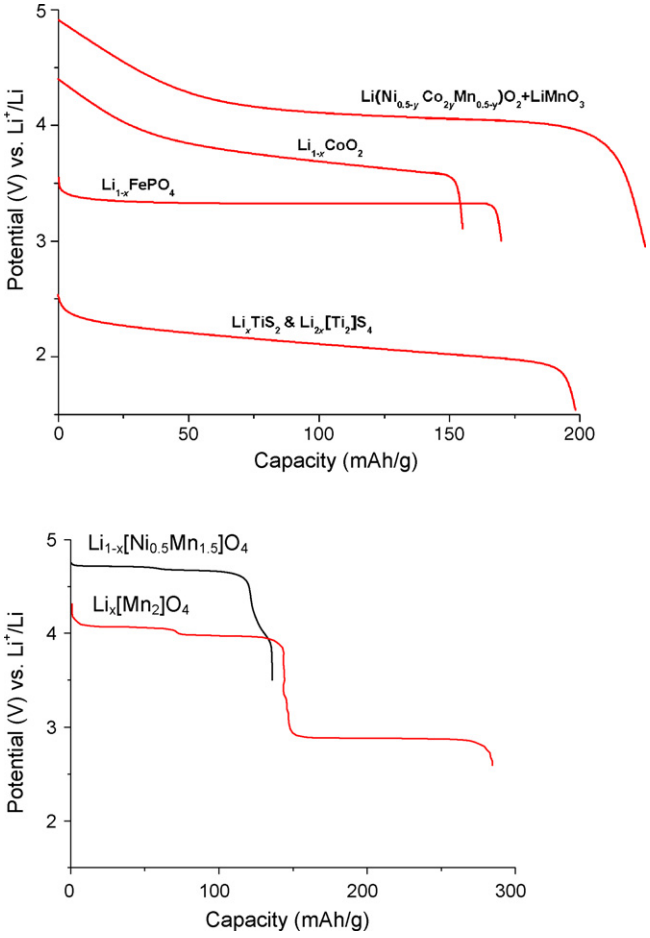

Fig. 10. Discharge voltage of several insertion-compound cathodes.

group of Shao-Horn [22], the efficiency of the Li/air cell for EES is not competitive.

The electrochemical potential μ_C of an S_8 cathode is so high that a Li anode is needed to give the Li/S battery a competitive energy density. However, unless there is a molecular shuttle in the electrolyte that suppresses dendrite formation on the Li anode, this strategy will require the introduction of a Li^+-ion solid-electrolyte separator with a Li^+-ion conductivity $\sigma_{Li} > 10^{-4}$ S cm^{-1} that can block Li dendrites from reaching the cathode without being reduced. In this case, the solid electrolyte only needs to be stable in a liquid-carbonate electrolyte contacting the electrodes on either side of it.

A third alternative also requires a solid Li^+-ion electrolyte with a $\sigma_{Li} > 10^{-4}$ S cm^{-1} that not only is not reduced by contact with a Li dendrite, but also is stable on the anode side against the carbonate electrolyte and against an aqueous solution on the cathode side. Fig. 6 shows the cell we designed to test the concept of an aqueous-solution cathode containing $Fe(NO_3)_3/Fe(NO_3)_2$. Two design challenges were: (1) to find sealing agents stable in both highly reducing and oxidizing environments and (2) to accommodate the electrode volume changes during cycling. We used a commercially available $Li_{1.3}Ti_{1.7}Al_{0.3}(PO_4)_3$ Li^+-ion solid electrolyte from OHARA that has the hexagonal NASICON structure of Fig. 7; it has a $\sigma_{Li} \approx 10^{-4}$ S cm^{-1}. First, we tested the use of pure water as the cathode; Fig. 8 shows that with pure water we obtained a poor efficiency for EES as in the case of a Li/air battery with an α-MnO_2 catalyst. On the other hand, Fig. 8 also shows that we obtained a flat discharge voltage of 3.75 V versus Li^+/Li^0 with the Li/Fe(III)/Fe(II)-aqueous-solution cell and a good recharge efficiency. However, the cycle life of the cell was poor because of the disintegration of the solid electrolyte in contact with an acid liquid cathode; and in an alkaline medium, we can expect $Fe(OH)_3$ to form. The origin of the solid-electrolyte failure is the existence of Ti(IV) in the electrolyte, which has a Ti(IV)/Ti(III) redox couple located at 2.5 eV below μ_{Li}, see Fig. 9. Visco et al. [23] of the Poly Plus Battery Co. have protected this solid electrolyte against reduction from contact with a Li dendrite by introducing a thin Li_3N solid separator layer on the anode side. However, it should be noted that use of this electrolyte in a Li/air battery causes failure if the carbon-substrate current collector for the cathode catalyst touches the electrolyte at the end of a discharge to a voltage below 2.5 eV versus Li^+/Li^0.

4. Conclusions

In order to develop Li-ion batteries of adequate energy density for EVs and grid EES at an acceptable cost, it will be necessary to go beyond present strategies that are based on insertion-compound cathodes. Fig. 10 shows the voltage profiles versus Li^+/Li^0 of the available insertion-compound cathodes. The step drop of 1 V in the output voltage of the $Li_{2x}[Mn_2]O_4$ cathode at $x = 0.5$ shows that oxide electrodes with a spinel framework have a capacity limited to 1 Li per 2 host cations, but the highest capacities that have been achieved thus far correspond to only 1 Li per host cation. The higher capacity of the C-$Ti_{0.9}Nb_{0.1}Nb_2O_7$ anode relative to the spinel $Li_4Ti_5O_{12}$ makes it competitive for a Li battery that supports a fast charge, *i.e.*, has no SEI layer on the anode, but to date a fast charge comes at the expense of a loss of full-cell voltage of

about 1.3 V. To increase the full-cell voltage, it will be necessary to develop an SEI layer on a carbon-based anode that will allow a fast charge that is safe unless the battery uses a Li anode with a Li^+-ion solid electrolyte as separator. Moreover, a cathode potential $\mu_C \approx 4.8$ eV below μ_{Li} is at the intrinsic limit of oxides as well as the decomposition limit of a liquid-carbonate electrolyte.

The use of a liquid cathode consisting of a redox couple in an aqueous electrolyte and a suitable Li^+-ion or Na^+-ion solid electrolyte would provide an alternative strategy that has been shown to be feasible and can be extended to include a flow-through cathode to increase further the capacity. However, exploitation of this strategy awaits identification of a suitable solid electrolyte with a $\sigma_{Li} > 10^{-4}$ S cm^{-1}.

Acknowledgments

This work was supported by the Assistant Secretary for Energy Efficiency and Renewable Energy, Office of Vehicle Technologies of the U.S. Department of Energy under contract no. DE-AC02-05CH11231, under the Batteries for Advanced Transportation Technologies (BATT) program. This work was also supported by the Robert A. Welch Foundation, Grant#F-1066.

References

[1] R. Fong, U. van Sacken, J.R. Dahn, J. Electrochem. Soc. 137 (1990) 2009–2013.
[2] S. Sinha, D.W. Murphy, Solid State Ionics 20 (1986) 81–84.
[3] W. Choi, A. Manthiram, Electrochem. Solid State Lett. 9 (2006) A245–A248.
[4] J.C. Hunter, J. Solid State Chem. 39 (1981) 142–147.
[5] Y.H. Huang, K.S. Park, J.B. Goodenough, J. Electrochem. Soc. 153 (2006) A2282–A2286.
[6] T. Ohzuku, A. Ueda, N. Yamamoto, J. Electrochem. Soc. 142 (1995) 1431–1435.
[7] J.T. Han, J.B. Goodenough, unpublished.
[8] M. Gasperin, J. Solid State Chem. 53 (1984) 144–147.
[9] Y. Kim, J.B. Goodenough, J. Phys. Chem. C 112 (2008) 15060–15064.
[10] J.B. Goodenough, Y. Kim, J. Solid State Chem. 182 (2009) 2904–2911.
[11] K. Mitzushima, P.C. Jones, P.J. Wiseman, J.B. Goodenough, Mater. Res. Bull. 15 (1980) 783–799.
[12] R. Gupta, A. Manthiram, J. Solid State Chem. 121 (1996) 483–491.
[13] S.B. Schougaard, J. Breger, M. Jiang, C.P. Grey, J.B. Goodenough, Adv. Mater. 18 (2006) 905–909.
[14] I. Saadoune, C. Delmas, Solid State Ionics 53 (1992) 370–375.
[15] Y. Wu, A. Manthiram, Electrochem. Solid State Lett. 9 (2006) A221–A224.
[16] D.Q. Liu, Y.H. Lu, J.B. Goodenough, J. Electrochem. Soc. 157 (2010) A1269–A1273.
[17] J. Liu, A. Manthiram, J. Phys. Chem. C 113 (2009) 15073–15079.
[18] D.Q. Liu, J.T. Han, M. Dontigny, K. Zaghib, J.B. Goodenough, J. Electrochem. Soc. 157 (2010) A770–A775.
[19] A.K. Padhi, K.S. Nanjundaswamy, C. Masquelier, J.B. Goodenough, J. Electrochem. Soc. 144 (1997) 2581–2586.
[20] A. Debart, A.J. Paterson, J. Bao, P.G. Bruce, Angew. Chem. Int. Ed. 47 (2008) 4521–4524.
[21] X. Ji, K.T. Lee, L.F. Nazar, Nat. Mater. 8 (2009) 500–506.
[22] Y. Lu, Z. Xu, H.A. Gasteiger, S. Chen, K. Hamad-Schifferli, Y. Shao-Horn, J. Am. Chem. Soc. 132 (2010) 12170–12171.
[23] S.J. Visco, E. Nimon, B. Katz, M. Chu, L. DeJonghe, Beyond Li-ion, A Strategy for Step-Change Improvement in Energy Density 5th Annual International Conference: Lithium Mobile Power 2009, Boston, November 12–13, 2009.